Supporting Information

Multifunctional MoS_2/Ni_9S_8/NF catalyst for synchronous desulfurization and hydrogen evolution by self-driven system

Jiangsu Key Laboratory of Advanced Catalytic Materials & Technology, School of Petrochemical Engineering, Changzhou University, Changzhou 213164, China. Email: gupeiyang0714@cczu.edu.cn (P. Gu)

1. Experimental section

1.1. Chemicals and reagents

All chemicals used in the experiment were of analytical grade and utilized without further purification. Sodium molybdate dihydrate ($Na_2MoO_4 \cdot 2H_2O$, 99%), nickel nitrate hexahydrate ($Ni(NO_3)_2 \cdot 6H_2O$, 98%), sodium hydroxide (NaOH, 96%), sodium sulfide nonahydrate ($Na_2S \cdot 9H_2O$, 44%), and potassium hydroxide (KOH, 85%) were obtained from Sinopharm Chemical Reagent Co., Ltd., Shanghai. Thioacetamide (CH_3CSNH_2, 99%) was sourced from Shanghai Haohong Biomedical Technology Co., Ltd., also in Shanghai. Nickel foam (NF) was supplied by Hefei Kejing Material Technology Co., Ltd.; carbon paper by Toray Corporation; and 20% Pt/C by Johnson Chemical Co., Ltd. The cation exchange membrane, Nafion 117, was a commercial product from Dupont China Holding Co., Ltd., while the 5 wt.% Nafion solution was obtained from Sigma Aldrich Trading Co., Ltd., Shanghai. Deionized water was

purified using a pure water purifier.

1.2. Catalyst synthesis

Pretreatment of NF: Prior to use, commercial nickel foam (NF) with a thickness of 0.16 cm was cut into rectangular pieces measuring 1.5 × 1.0 cm^2. These pieces were then ultrasonically treated in a 3.0 M HCl solution for 30 minutes, followed by thorough rinsing with distilled water and ethanol to remove surface impurities.

Synthesis of MoS_2/Ni_9S_8/NF: The MoS_2/Ni_9S_8/NF catalyst was synthesized using a simple one-step hydrothermal method. In this process, 0.466 mmol of $Na_2MoO_4 \cdot 2H_2O$, 3.0 mmol of C_2H_5NS, and 0.0466 mmol of $Ni(NO_3)_2 \cdot 6H_2O$ were dissolved in 30 mL deionized water under ultrasonication to form a uniform solution. The solution was then transferred into a Teflon-lined stainless steel autoclave reactor (50 mL), with the NF immersed vertically. The reactor was heated to 180 °C for 18 h. After cooling to room temperature, the NF was carefully removed and rinsed multiple times with deionized water and ethanol to remove remaining salts and organic matter. Finally, it was dried at 60 °C for 2 hours in an oven to obtain MoS_2/Ni_9S_8/NF. The mass loading of MoS_2/Ni_9S_8 on the NF support is approximately 15.52 mg/cm^2.

Synthesis of Ni_9S_8/NF, Mo-Ni_9S_8/NF and Pt-C/CP: In comparison to the preparation of MoS_2/Ni_9S_8/NF, the Ni_9S_8/NF electrodes were also synthesized under identical conditions without the presence of a molybdenum source.

The synthesis processes of Mo-Ni_9S_8/NF electrodes are similar to those of MoS_2/Ni_9S_8/NF, except for the absence of an external Ni source. In this case, the

cleaned NFs are immersed into the solution to provide the Ni source and serve as substrates for products.

Synthesis of Pt-C/CP: 4 mg of Pt/C powder (20%) was evenly dispersed in a mixture of 375 μL of deionized water, 125 μL of methanol and 20 μL of Nafion. Then, the inks were evenly dripped onto carbon paper and the electrodes were dried at 80 °C for 12 h. The obtained electrode was denoted Pt-C/CP.

1.3. Characterization

The structure of all synthesized catalysts were characterized using X-ray diffraction (XRD) patterns. The diffraction patterns were recorded on a Bruker D8 Advance X-ray spectrometer equipped with a 2D detector (Cu Kα, λ=1.5406 Å, ranging from 10-80°, at a scan rate of 0.1°/s). Microstructures were characterized using a scanning electron microscope (SEM, S-4800, Hitachi, Japan) and transmission electron microscopy (TEM, FEI Tecnai G2 F20, USA). XPS measurements were performed on an Escalab 250Xi photoelectron spectrometer at a vacuum level of 2.4×10^{-10} mbar using a monochromatic Al Ka x-ray beam (1486.60 eV). UV-Vis absorption spectra were obtained using a Cary 5000 spectrophotometer (Varian).

1.4. Electrochemical measurement

All electrochemical and battery measurements were conducted in triplicate to minimize measurement errors.

Three-electrode testing system: the SOR, HER, ORR, OER performance were firstly evaluated using traditional three-electrode system through Electrochemical Workstation (CHI660E, CH Instruments, Inc. Shanghai), where the prepared sample,

Pt foil and Hg/HgO (in alkaline electrolytes) and Ag/AgCl (in acid electrolytes) were act as the working electrode, counter electrode, and reference electrode, respectively. In general, Electrochemical impedance spectroscopy (EIS) measurements were conducted at onset potentials from 0.1~100 kHz with an AC amplitude of 5.0 mV at 0.3 V vs. RHE. A 90% iR compensation was performed in the measurements to compensate for electrolyte resistance. All potential values were calibrated to the reversible hydrogen electrode (RHE) using the Nernst equations S1 and S2:

$$E_{RHE} = E_{Ag/AgCl} + 0.059 \times pH + 0.197 \quad (S1)$$

$$E_{RHE} = E_{Hg/HgO} + 0.059 \times pH + 0.098 \quad (S2)$$

Chronopotentiometry tests were carried out at a current density of 100 mA cm^{-2}. During the test, we maintained a stable working environment by replacing the electrolyte every 24 hours. For SOR, the cathodic electrolyte consisted of 1.0 M NaOH and 1.0 M Na_2S. Linear sweep voltammetry (LSV) measurements ranged from -0.9 to -0.2 V (versus Hg/HgO) at a sweep rate of 5.0 mV s^{-1}; For HER, 1.0 M NaOH aqueous solution was used as electrolytes for the test. The LSV curves were performed from -0.9 to -1.5 V (vs. Hg/HgO); For ORR, a glassy carbon electrode (GCE, Ø 2 mm) was used as the working electrode and 0.1 M KOH was used as the electrolyte. Prior to electrochemical testing, the glassy carbon was polished. The MoS_2/Ni_9S_8/NF catalysts (4.0 mg) were then uniformly dispersed in a mixture of 375 μL deionized water, 125 μL methanol, and 20 μL Nafion, followed by 30 minutes of ultrasonic treatment to create a homogeneous ink. The ink was applied to the glass carbon electrode and air-dried at room temperature. ORR activity was evaluated through LSV at a scan rate of

5.0 mV s^{-1}.

Two-electrode testing system: The SOR||HER system for simultaneous desulfurization and hydrogen production was constructed using two MoS_2/Ni_9S_8/NF electrodes as both the cathode and anode. A mixture of 1.0 M NaOH and 1.0 M Na_2S was served as the anolyte, while 1.0 M NaOH solution utilized as the catholyte. The cathode and anode compartments were separated by a Nafion 117 membrane. Electrolysis tests were conducted on a CHI660E electrochemical workstation, with polarization curves measured at a scan rate of 10.0 mV s^{-1} along with iR compensation.

Fabrication of aqueous rechargeable Zn-air batteries (ZABs): The Zn-air battery was fabricated using powder catalyst (MoS_2/Ni_9S_8) as the air cathode, a polished zinc plate with a thickness of 300 μm as the anode, and a 6.0 M KOH + 0.2 M $Zn(OAc)_2$ solution as the electrolyte in a custom-built setup for Zn-air batteries.

Self-driven coupling system: To establish a self-driven SOR||HER coupling system, the obtained MoS_2/Ni_9S_8/NF catalyst was used as the cathode in a Zn-air battery and served dual functions as both the anode and cathode in the SOR||HER system. The Zn-air battery supplies the necessary power for the SOR||HER system. Furthermore, the drainage method was employed to collect hydrogen rate data for the self-driven system. Specifically, hydrogen was carefully collected at ten-minute intervals to analyze the relationship between hydrogen yield and system runtime. The rate of hydrogen production (v, mmol/min/$g_{catalyst}$) was calculated for the catalyst-loaded Zn-air battery using the following equation S3:

$$v = v_{mmol}/m \quad \text{(S3)}$$

Where v_{mmol} (mmol/min) represents the molar rate of hydrogen production during system operation, and m (g) is the mass of the catalyst used for driving the Zn-air battery.

Electrochemical active surface area (ECSA) calculation: The electrochemically active surface area (ECSA) was calculated using the double-layer capacitance method. Specifically, the double-layer capacitance (C_{dl}) was estimated by analyzing the scan rate-dependent double-layer charging currents in the non-Faradaic region. To obtain the C_{dl} value, cyclic voltammetry (CV) measurements were performed in the non-Faradaic region at different scan rates of 2.0, 4.0, 6.0, 8.0, and 10.0 mV s^{-1}. The C_{dl} value was calculated using the following equation S4:

$$C_{dl} = \frac{j_{anodic} - j_{cathodic}}{v} = \frac{\Delta j}{v} \quad \text{(S4)}$$

where j_{anodic} and $j_{cathodic}$ are the anodic and cathodic current density, respectively, recorded at the middle of the selected potential range, and v is the scan rate. Generally, the C_{dl} value was estimated by plotting the line of Δj vs. scan rate, the slope of which gives the C_{dl} value.

The ECSA was then calculated from the C_{dl} using the specific capacitance value for a flat standard with a real surface area of 1 cm^2. The calculation equation S5 for ECSA is as follows:

$$E_{ECSA}^{catalyst} = \frac{C_{dl}^{catalyst}(mF \cdot cm^{-2})}{C_{dl}^{NF}(mF \cdot cm^{-2})\ per\ cm_{ECSA}^{2}} \quad \text{(S5)}$$

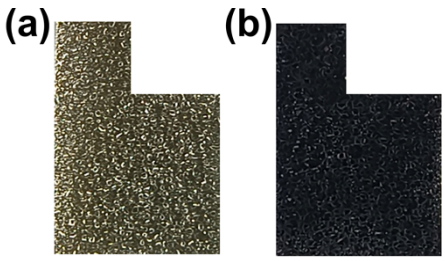

Figure S1 The photograph of (a) bare NF and (b) MoS_2/Ni_9S_8/NF.

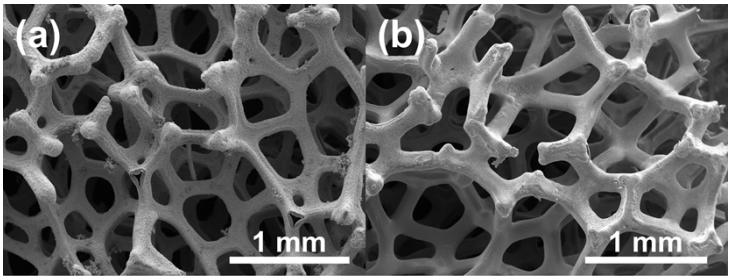

Figure S2 Low-magnification SEM images of (a) Ni_9S_8/NF and (b) Mo-Ni_9S_8/NF.

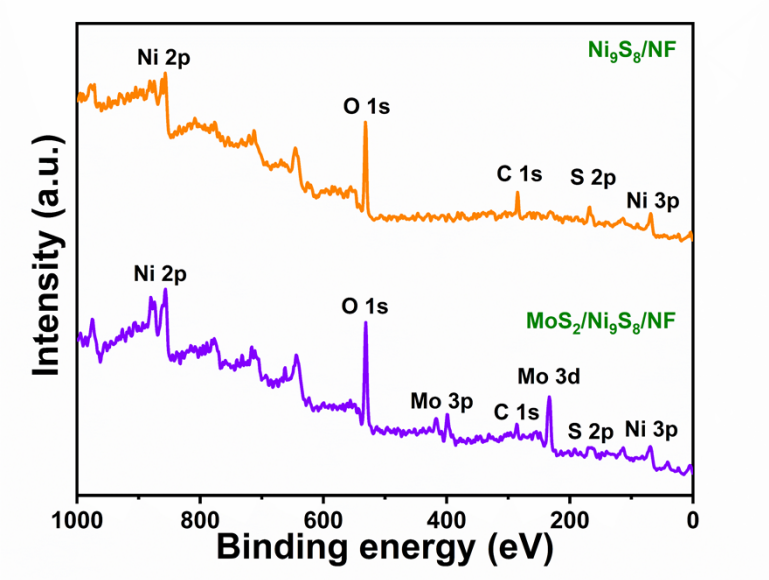

Figure S3 Full-survey XPS spectrum of the MoS_2/Ni_9S_8/NF and Ni_9S_8/NF catalyst.

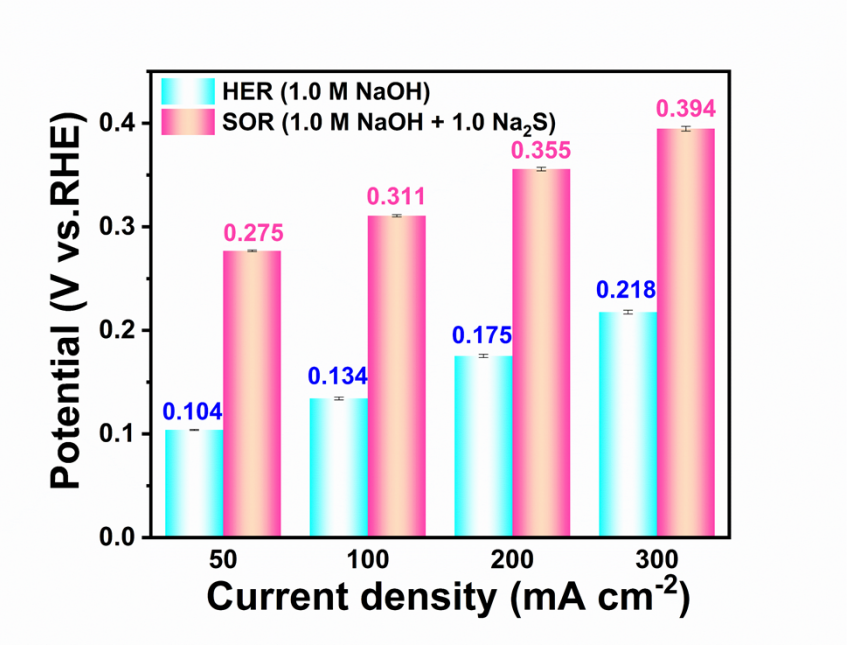

Figure S4 Potential comparison between HER and SOR based on MoS_2/Ni_9S_8/NF.

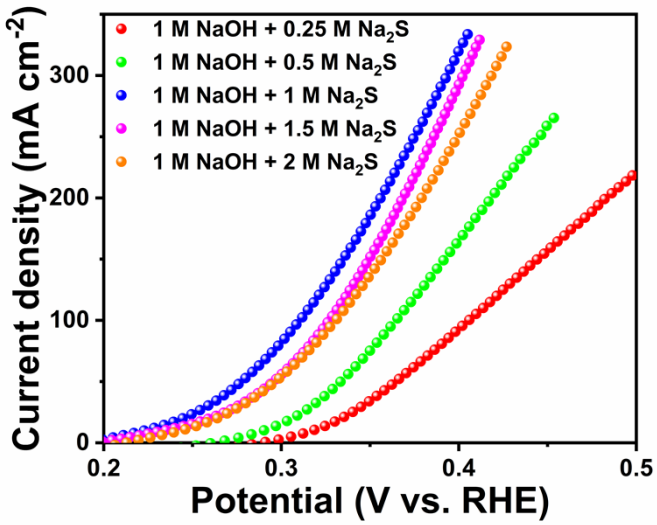

Figure S5 LSVs of MoS_2/Ni_9S_8/ NF for SOR in 1.0 M NaOH with various concentrations of Na_2S.

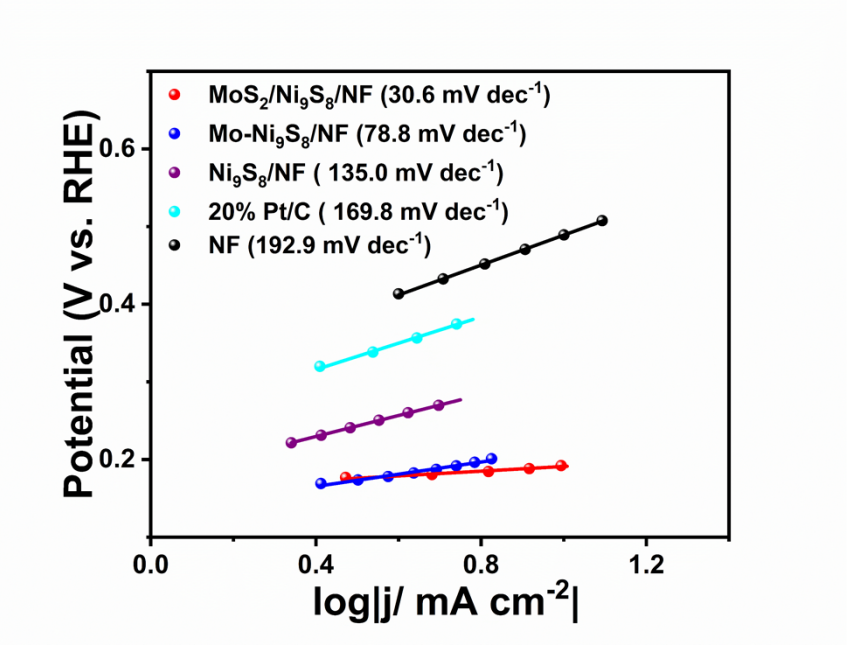

Figure S6 Comparison of Tafel slopes of MoS_2/Ni_9S_8/NF, Mo-Ni_9S_8/NF, Ni_9S_8/NF, 20% Pt/C, and NF for SOR.

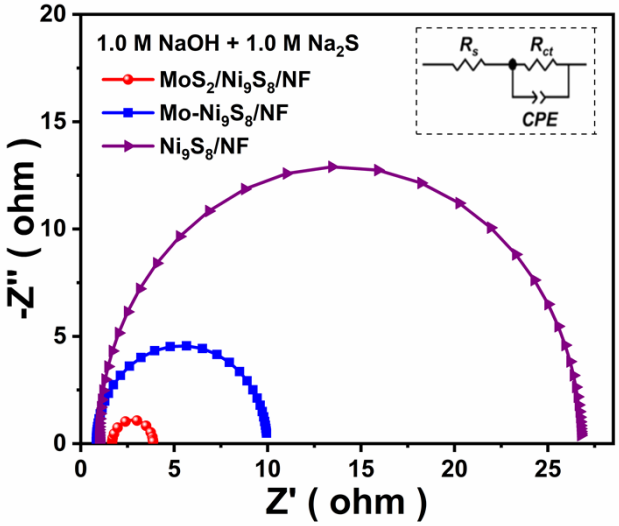

Figure S7 Nyquist plots of MoS_2/Ni_9S_8/NF, Mo-Ni_9S_8/NF, and Ni_9S_8/NF for SOR.

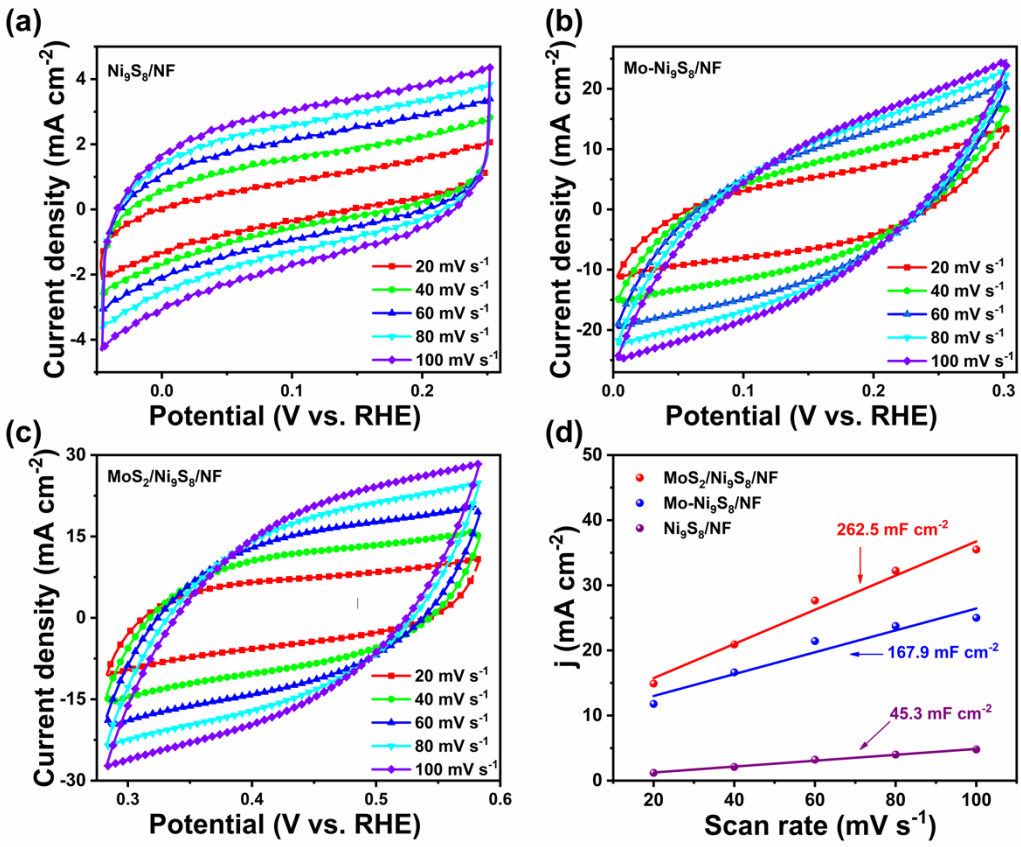

Figure S8 CV curves of (a) Ni_9S_8/NF, (b) Mo-Ni_9S_8/NF, and (c) MoS_2/Ni_9S_8/NF in 1.0 M Na_2S + 1.0 M NaOH; and (d) Plots of current density versus the scan rate from CVs under different scan rates.

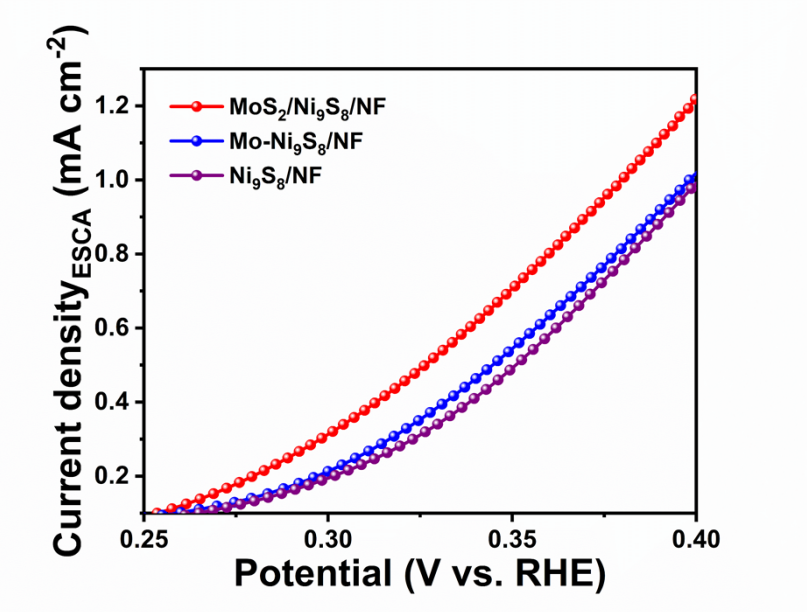

Figure S9 SOR LSV curves of MoS_2/Ni_9S_8, Mo-Ni_9S_8/NF, and Ni_9S_8/NF normalized by the electrochemical active surface area.

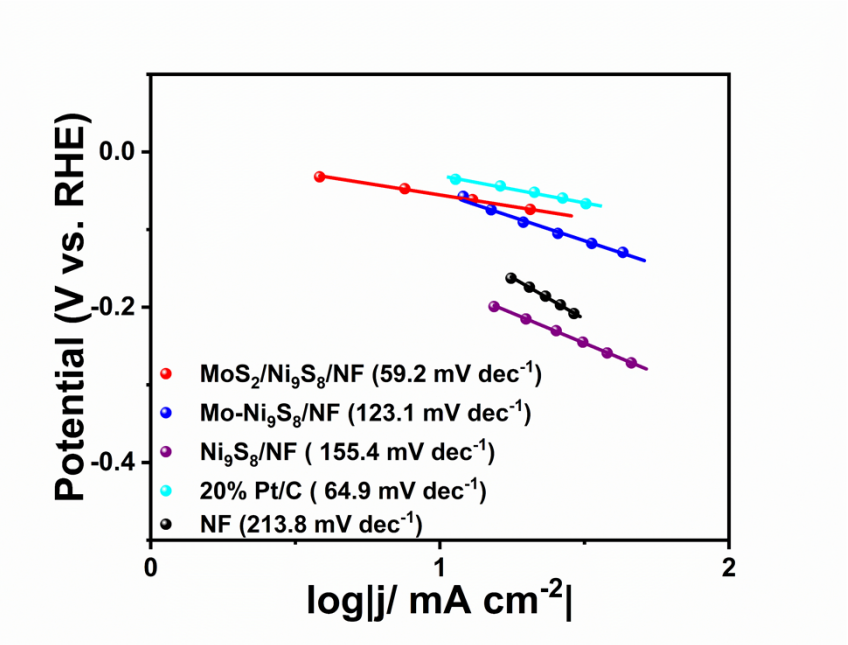

Figure S10 Comparison of Tafel slopes of MoS_2/Ni_9S_8/NF, Mo-Ni_9S_8/NF, Ni_9S_8/NF, 20% Pt/C, and NF for HER.

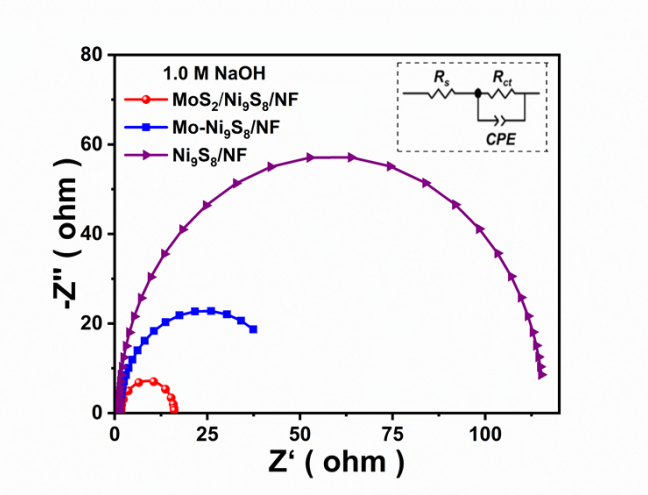

Figure S11 Nyquist plots of MoS_2/Ni_9S_8/NF, Mo-Ni_9S_8/NF, and Ni_9S_8/NF for HER.

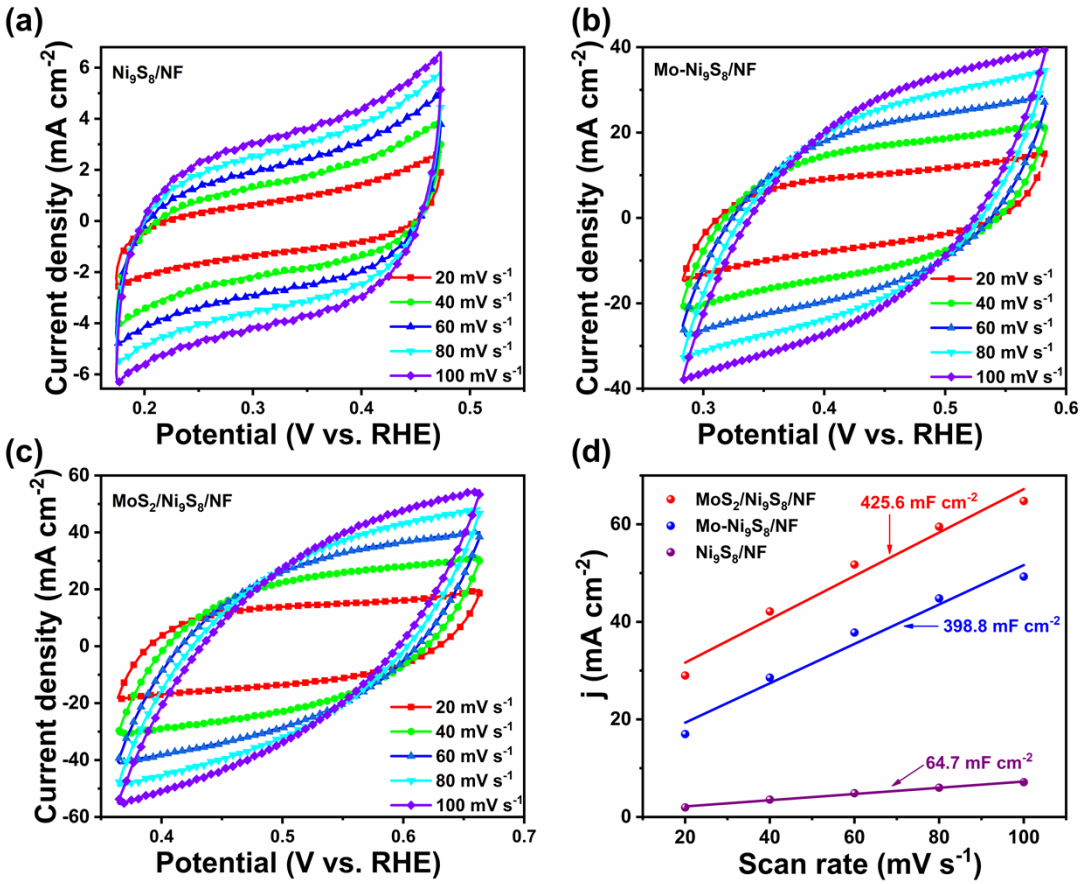

Figure S12 CV curves of (a) Ni_9S_8/NF, (b) Mo-Ni_9S_8/NF, and (c) MoS_2/Ni_9S_8/NF in 1.0 M NaOH; and (d) Plots of current density versus the scan rate from CVs under different scan rates.

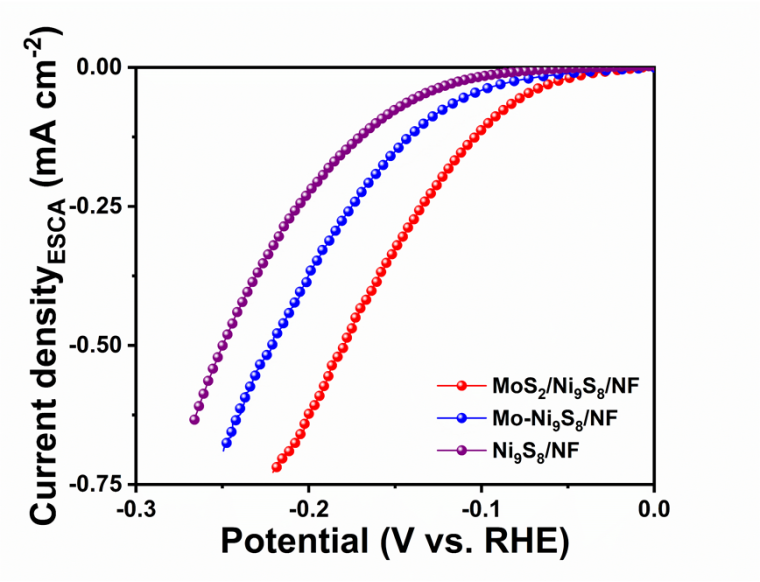

Figure S13 HER LSV curves of MoS_2/Ni_9S_8, Mo-Ni_9S_8/NF, and Ni_9S_8/NF normalized by the electrochemical active surface area.

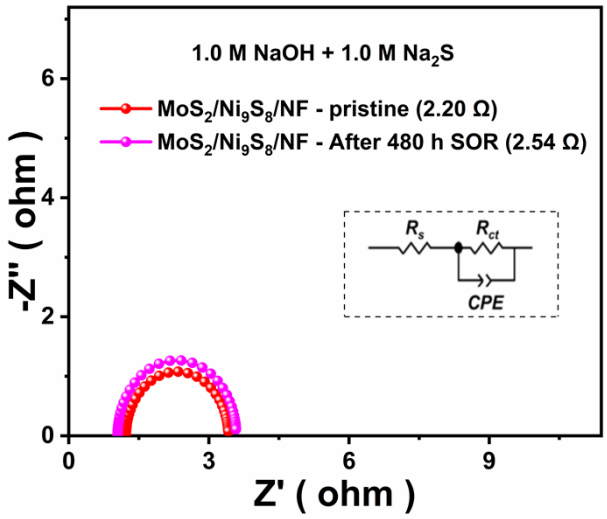

Figure S14 Comparison of the conductivity of pristine MoS_2/Ni_9S_8/NF before and after 480 hours for SOR.

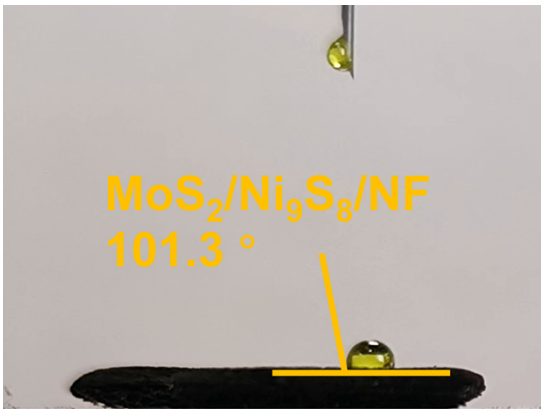

Figure S15 Contact angle measurements of sulfur droplets on MoS_2/Ni_9S_8/NF.

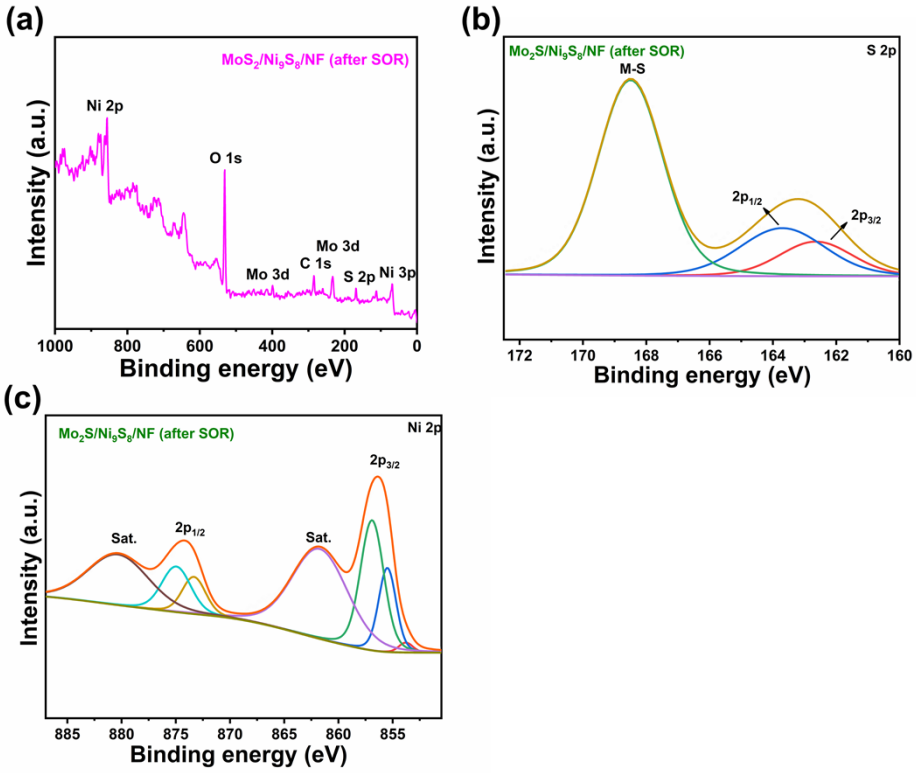

Figure S16 (a) Full-survey XPS, (b) S 2p, (c) Ni 2p spectra of the MoS_2/Ni_9S_8/NF after long-term stability tests for the SOR.

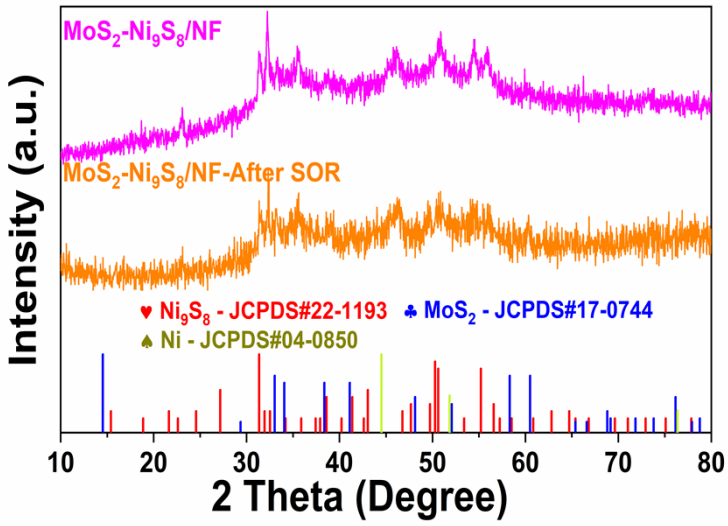

Figure S17 XRD patterns of MoS_2/Ni_9S_8/NF before and after long-term stability tests for SOR.

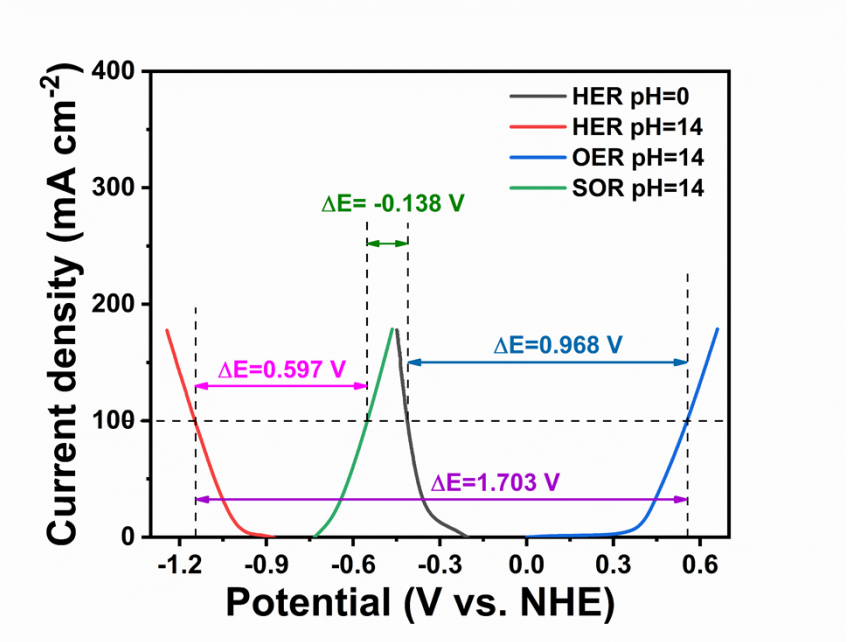

Figure S18 The polarization curves of the corresponding catalytic reaction based on NHE (using the absolute value of the current density) in a three-electrode test.

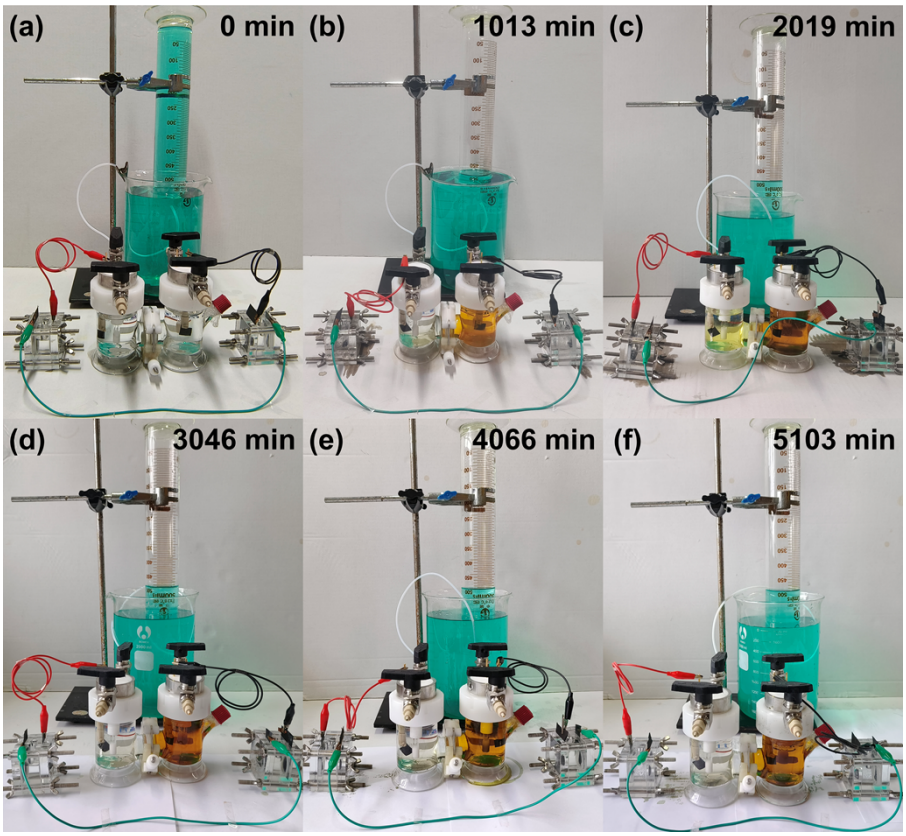

Figure S19 Pictures of the system producing hydrogen over (a) 0 min, (b) 1013 min, (c) 2019 min, (d) 3046 min, (e) 4066 min, and (f) 5103 min.

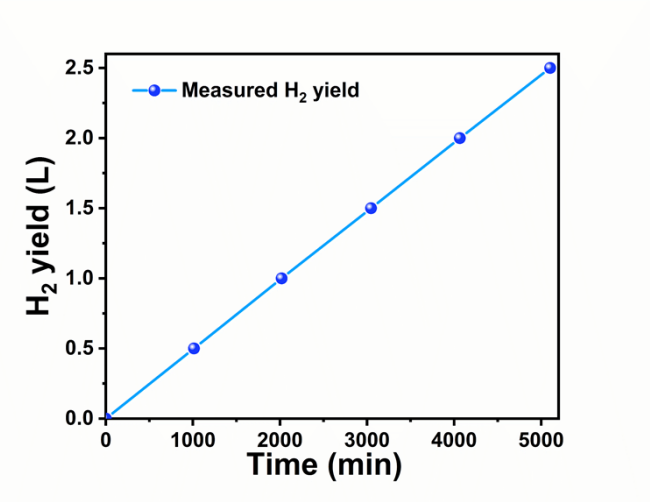

Figure S20 The variation regularity of the total amount of hydrogen generated in the self-driven system with the reaction time.

Video1.mp4

Video S1 Video of small fans powered in series by Zn-air battery.

Video 2.mp4

Video S2 Video of hydrogen production at different times in the self-driven system.

Table S1. A comparison of MoS_2/Ni_9S_8/NF with reported electrodes in SOR performance.

Catalyst	Potentials (mV) at different current densities ($mA \cdot cm^{-2}$)		Reference
	10	**100**	
MoS_2/Ni_9S_8/NF	**277**	**311**	**This work**
NiSe/NF[1]	-	490	Appl. Catal. B Environ. 2023, 324, 122255
CoNi@NGs[2]	-	500	Energy Environ. Sci., 2020, 13, 119
Ni-MoS_2/SM[3]	350	-	Energy Environ. Mater. 2023, 0, e12644
NiS_2[4]	410	-	Adv. Funct. Mater. 2021, 31, 2101922
A/C S-Pd NSA/NF[5]	-	470	Small. 2023, 19, 2207852
WS_2-NSs[6]	480	-	Angew. Chem. Int. Ed. 2021, 60, 21550 – 21557
Co-Ni_3S_2/NF[7]	300	590	Chem. Eng. J. 2022, 433, 134472
Cu_2S/NF[8]	-	440	Green Chem. 2021, 23, 6975–6983
TAP@Ni_3S_2/NF[9]	-	480	Applied Surface Science 605 (2022) 154756

Table S2. A comparison of MoS_2/Ni_9S_8/NF with reported electrodes in HER performance.

Catalyst	Potentials (mV) at different current densities ($mA \cdot cm^{-2}$)		Reference
	10	**100**	
MoS_2/Ni_9S_8/NF	**56**	**143**	**This work**
Co_3S_4/NF[10]	-	193	Adv. Funct. Mater. 2023, 33, 2212183
Mo-Co-S /NF[11]	-	350	Inorg. Chem. Front. 2023, 22, 6728-6737
Ni-MoS_2/SM[3]	109	-	Energy Environ. Mater. 2023, 0, e12644
Co@N-CNTs/CC[12]	67	-	Chinese Chem.Lett. 2023, 23, 122255
WS_2-NSs[6]	214	-	Angew. Chem. Int. Ed. 2021, 60, 21550 – 21557
Co-Ni_3S_2/NF[7]	192	-	Chem. Eng. J. 2022, 433, 134472
Cu_2S/NF[8]	-	420	Green Chem. 2021, 23, 6975–6983
CuCoS/CC[13]	-	214	J. Mater. Chem. A. 2023,11, 2218-2224

References

1. C. Duan, C. Tang, S. Yu, L. Li, J. Li and Y. Zhou, *Applied Catalysis B: Environmental*, 2023, **324**, 122255.
2. M. Zhang, J. Guan, Y. Tu, S. Chen, Y. Wang, S. Wang, L. Yu, C. Ma, D. Deng and X. Bao, *Energy & Environmental Science*, 2020, **13**, 119-126.
3. F. Liu, X. Cai, Y. Tang, W. Liu, Q. Chen, P. Dong, M. Xu, Y. Tan and S. Bao, *Energy & Environmental Materials*, 2024, **7**, e12644.
4. S. Zhang, Q. Zhou, Z. Shen, X. Jin, Y. Zhang, M. Shi, J. Zhou, J. Liu, Z. Lu, Y.-N. Zhou and H. Zhang, *Advanced Functional Materials*, 2021, **31**, 2101922.
5. W. Wang, Q. Mao, K. Deng, H. Yu, Z. Wang, Y. Xu, X. Li, L. Wang and H. Wang, *Small*, 2023, **19**, 2207852.
6. L. Yi, Y. Ji, P. Shao, J. Chen, J. Li, H. Li, K. Chen, X. Peng and Z. Wen, *Angewandte Chemie International Edition*, 2021, **60**, 21550-21557.
7. Y. Li, Y. Duan, K. Zhang and W. Yu, *Chemical Engineering Journal*, 2022, **433**, 134472.
8. Y. Pei, J. Cheng, H. Zhong, Z. Pi, Y. Zhao and F. Jin, *Green Chemistry*, 2021, **23**, 6975-6983.
9. L. Jin, C. Chen, L. Hu, X. Liu, Y. Ding, J. He, H. Li, N. Li, D. Chen, Q. Xu and J. Lu, *Applied Surface Science*, 2022, **605**, 154756.
10. Z. Xiao, C. Lu, J. Wang, Y. Qian, B. Wang, Q. Zhang, A. Tang and H. Yang, *Advanced Functional Materials*, 2023, **33**, 2212183.
11. X. Tang, Y. Zhang, F. Wu, B. Li, J. Wang, X. Li, R. Rao, J. Hu, D. Xiao and T.

Gao, *Inorganic Chemistry Frontiers*, 2023, **10**, 6728-6737.

12. H. Wang, B. Wang, H. Yu, K. Deng, Y. Xu, X. Li, Z. Wang and L. Wang, *ACS Applied Nano Materials*, 2023, **6**, 10863-10871.

13. H. Yu, W. Wang, Q. Mao, K. Deng, Y. Xu, Z. Wang, X. Li, H. Wang and L. Wang, *Journal of Materials Chemistry A*, 2023, **11**, 2218-2224.